Exchange interaction of magnetic impurities in a biased bilayer phosphorene nanoribbon

Moslem Zare* and Ebrahim Sadeghi
Department of Physics, Yasouj University, Yasouj, Iran 75914-353, Iran

(Received 29 July 2018; published 2 November 2018)

We study the Ruderman-Kittel-Kasuya-Yosida (RKKY) interaction between local magnetic moments in zigzag bilayer phosphorene nanoribbons (ZBLPNRs) under a perpendicular electric field. We evaluate the spatial and electric field dependency of the static spin susceptibility in real space in various configurations of the magnetic impurities at zero temperature. For large distances, the RKKY interaction falls off as R^{-5} for moments located on the zigzag edge, whereas for those placed at interstitial sites it decays as R^{-3}. In the presence of a large bias potential, a beating pattern of the RKKY oscillations occurs when two magnetic impurities are located inside the ZBLPNR. The electrically tunable RKKY interaction of ZBLPNRs is expected to have important consequences on the spintronic application of a biased ZBLPNR. The electronic properties of ZBLPNRs in the presence of gate voltage are also obtained. In comparison to other two-dimensional materials such as graphene, silicene, etc., the ZBLPNR has two nearly degenerate quasiflat edge modes at the Fermi level, isolated from the bulk states. The band-gap modulation of ZBLPNRs by the ribbon width and perpendicular electric field is investigated. Due to the existence of these quasiflat bands at the Fermi level, in the absence of an electric field, a sharp peak in the RKKY interaction is seen. As is shown, the signatures of these unique quasiflat edge modes in ZBLPNRs could be explored by using the RKKY interaction.

DOI: 10.1103/PhysRevB.98.205401

I. INTRODUCTION

Black phosphorus (BP) monolayer, called phosphorene, has emerged as a promising material in the field of optoelectronics and magnetoelectronics of two-dimensional (2D) systems [1–7]. Phosphorene has a puckered honeycomb structure due to the sp^3 hybridization [8–14]. Its conventional unit cell consists of four atoms with the lattice constants $a_x = 3.3$ Å and $a_y = 4.63$ Å in x (zigzag) and y (armchair) directions, respectively. The structural anisotropy of phosphorene ensures that its thermal, electrical, and optical properties [2,12,14,15] have a high degree of anisotropy. Charge carriers in phosphorene exhibit exceptionally high carrier mobilities at room temperature, $\sim$1000 cm^2 V^{-1} s^{-1} [1,2], which demonstrates strongly anisotropic behavior in the phosphorene-based field-effect transistor with a high on/off ratio of $\sim 10^4$ [2]. Moreover, by changing the number of layers and applying strain and an external field, the direct band gap of BP multilayer systems can be varied, spanning the losing gap between graphene and other 2D materials [2,15–19]. As the layer number strongly affects the physical properties of 2D black phosphorus multilayers, it is of both fundamental and practical interest to study the effect of interlayer coupling on these physical properties. In this regard, bilayer phosphorene (BLP) is an appropriate candidate that can provide basic information on this coupling effect.

In the past decade, dilute semiconductors have emerged as a hot topic of research due to their unique and new functionalities. In this regard, utilizing phosphorene may lead to the next generation of spintronic devices based on spin degrees of freedom [20,21].

The nonmagnetic nature of the pristine semiconductor phosphorene limits its applications in the field of magnetoelectronics and spintronics. Phosphorene can be magnetized in several ways, such as doping with nonmagnetic adatoms [22–24], edge cutting [25–29], or inserting atomic defects and vacancies on phosphorene [21,30,31]. Phosphorene nanoribbons (PNRs) with bare zigzag edges are antiferromagnetic semiconductors [26]. This magnetization also opens a significant direct band gap (about 0.7 eV), which transforms the metallic PNRs into semiconductors ones.

The most effective approach to induce magnetization with high Curie temperature is the adsorption or substitutional doping of 3d transition-metal atoms on phosphorene [32–36]. As transition-metal atoms interact much more strongly with phosphorene compared with other two-dimensional materials such as graphene, it becomes more probable to turn pristine phosphorene into a ferromagnetic or antiferromagnetic material [34]. The strength of these created magnetic moments depends on the metal species, and the result can be tuned by the applied strain [35–39].

The Ruderman-Kittel-Kasuya-Yosida (RKKY) exchange interaction [40–42], a fundamental interaction for spintronic applications, is mediated by a background of conduction electrons of the host material. It is the most important mechanism of coupling between magnetic impurity dopants in metals and semiconductors. From an application point of view, this interaction can lead a magnetically doped system to interesting phases such as ferromagnetic [43–48], antiferromagnetic [49,50], spiral [51,52], and spin-glass [53–55]. In addition to the practical importance of the RKKY interaction in the possible magnetic phases of semiconductors, it can provide

*mzare@yu.ac.ir

information about the intrinsic properties of the materials since this coupling is proportional to the spin susceptibility of the host system. While this interaction falls off by R^{-D}, where D is the dimension of the system [56,57], it oscillates with the Fermi wave vector originating from the Friedel oscillations. In systems with a multiband structure [57] or with spin polarization [58], these oscillations become more complicated than a monotonic oscillation with $\sin(2k_F R)$ behavior, where k_F is the wave vector of the electrons (holes) at the Fermi level, and R is the distance of two magnetic impurities. Moreover, it has been shown that the magnitude of the RKKY interaction can be severely affected by the density of states (DOS) at the Fermi energy [52,56]. In addition, it can be sensitive to the direction of the distance vector between impurities in materials such as graphene [56,59] due to the bipartite nature of the honeycomb sublattice. In materials with Rashba spin-orbit coupling, the spin response of the system to the magnetic impurity depends on the direction of the magnetic moment [60], and as a result the RKKY interaction becomes anisotropic [52].

RKKY interactions in a nanoribbon of two-dimensional lattices has attracted a great deal of attention in the area of condensed-matter physics [51,61–63]. Recently, in a detailed study it was shown that the topological phase transition in a zigzag silicene nanoribbon can be probed by using the RKKY interaction [51]. In another work, it was concluded that the RKKY interaction in the bulk phosphorene monolayer is highly anisotropic, and the magnetic ground state of two magnetic adatoms can be tuned by changing the spatial configuration of impurities as well as varying the chemical potential [62]. Duan *et al.* also studied the effect of strain on the magnetic impurity interactions in phosphorene [63]. Very recently, the effect of tensile strain on the RKKY interaction in a biased monolayer phosphorene nanoribbon was studied numerically [64]. It was shown how one could isolate the edge state from that of the bulk contribution, using the RKKY interaction by tuning the external gate potential.

In this paper, we present the Green's-function technique for derivation of the RKKY interaction in a biased bilayer phosphorene nanoribbon. Also, we show that by changing the perpendicular electric field due to the band-structure change, one can drastically alter the interaction between impurities, which can be a great way to control magnetic properties via an electric field.

This paper is organized as follows. In Sec. II, we introduce a tight-binding model Hamiltonian for biased bilayer phosphorene, and then we calculate the band spectrum of a zigzag bilayer phosphorene nanoribbon (ZBLPNR) under a vertical electric field. Here we introduce the theoretical framework that will be used in calculating the RKKY interaction from the real-space Green's function. In Sec. III, we discuss our numerical results for the proposed magnetic doped ZBLPNR in the presence of a perpendicular electric field. Finally, our conclusions are summarized in Sec. IV.

II. THEORY AND MODEL

As the Bernal stacking configuration of two phosphorene layers, coupled via the van der Waals interaction, is energetically the most stable form of bilayer phosphorene [65,66], we consider an AB stacked ZBLPNR as shown in Fig. 1. In the presence of a uniform perpendicular electric field, low-energy carriers in BLP are described by the following tight-binding (TB) Hamiltonian [64,67,68]:

$$H = \sum_i V_i c_i^\dagger c_i + \sum_{i \neq j} t_{ij}^{\parallel} c_i^\dagger c_j + \sum_{i \neq j} t_{ij}^{\perp} c_i^\dagger c_j, \qquad (1)$$

where the summation runs over all lattice sites of the system. $c_i^\dagger$ (c_j) is the creation (annihilation) operator of an electron at site i (j), V_i is the on-site energy at site i, and $t_{ij}^{\parallel}$ ($t_{ij}^{\perp}$) is the intralayer (interlayer) hopping energy between sites i and j. The relevant hopping parameters considered by Li *et al.* [64] are two in-plane hopping terms ($t_1 = -1.21$ eV, $t_2 = 3.18$ eV) and an interlayer term $t_3 = 0.22$ eV. In the presence of a perpendicular electric field E, the four atomic sublayers in BLP will earn different on-site electrostatic potentials in the form of $V_1 = (1/2 + \epsilon)V$, $V_2 = (1/2 - \epsilon)V$, $V_3 = (-1/2 + \epsilon)V$, and $V_4 = (-1/2 - \epsilon)V$, where $V = eEd$ is the electrostatic potential energy difference between the top and bottom phosphorene layers, with e the elementary charge, d the interlayer separation, and $\epsilon = 0.202$ is a linear scaling factor that accounts for the sublayer dependence of the on-site electrostatic potential [69].

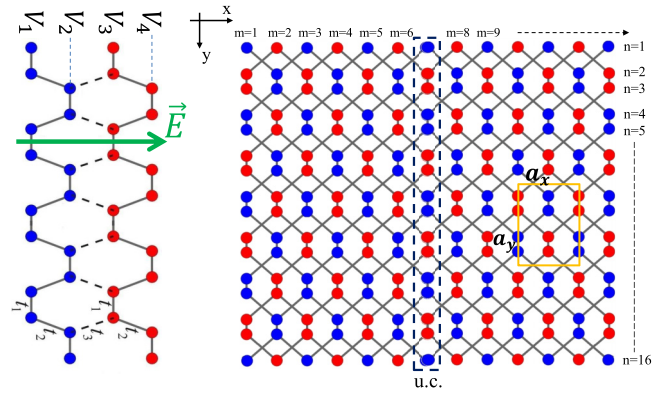

FIG. 1. Sketch of the side view (left) and top view (right) of the two-dimensional lattice structure of a zigzag bilayer black phosphorus nanoribbon with $N = 16$ in the presence of a perpendicular electric field $\vec{E}$. Blue and red circles correspond to atoms located in the bottom and top layers, respectively. The relevant hopping terms considered in Hamiltonian (1) are two in-plane hopping terms ($t_1 = -1.21$ eV, $t_2 = 3.18$ eV) and an interlayer term ($t_3 = 0.22$ eV). The orange rectangle represents the unit cell of bilayer phosphorene with the lattice constants a_x and a_y, and the dashed rectangle denotes the unit cell (u.c.) in the calculation of nanoribbon.

The geometry of a ZBLPNR with zigzag edges is illustrated in Fig. 1. Its conventional unit cell consists of eight atoms with lattice constants a_x and a_y in the x (zigzag) and y (armchair) directions, respectively, which are exactly equal to the monolayer phosphorene lattice constants. Here, the unit cell used in the tight-binding calculations of the ZBLPNR (dashed rectangle), containing N atoms, is also indicated. The width of the respective unit cell is a_x. For simplicity, as shown in this figure, each atom is labeled with a set (m, n), where m, n represent the x and y coordinates of the lattice points. In our analysis, we consider the two magnetic impurities located at (m_1, n_1) and (m_2, n_2) sites of the nanoribbon (following

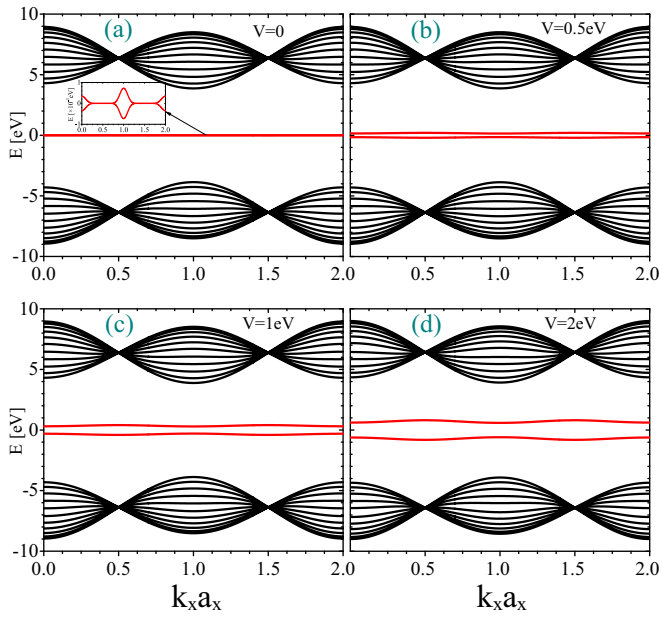

FIG. 2. Energy bands for a ZBLPNR of $N = 24$ with periodic boundary conditions in one direction (x) for several values of the external electric potential V, in which k_x is the wave vector parallel to the zigzag direction.

the notations of Fig. 1), in which we define edge and bulk configurations for magnetic impurities located at the edge or inside of the ZBLPNR, respectively. In this ribbon geometry, it is easy to find the energy dispersion with the periodic boundary condition along the two ribbon zigzag edges in the x direction. Due to the translational invariant along the ribbon edges (x), the momentum in the x direction is a good quantum number. To study the band-structure properties provided by our tight-binding model, we find its **k** space form as $\sum_{\mathbf{k}} \psi^{\dagger}_{\mathbf{k}} H_k \psi_{\mathbf{k}}$. Applying Bloch's theorem, performing the Fourier transformation along the x direction, the Hamiltonian in **k** space can be written as

$$H_k = H_{AA} + H_{BB} + H_{AB} e^{-ik_x a_x} + H^{\dagger}_{AB} e^{ik_x a_x}, \qquad (2)$$

where H_{AA} and H_{BB} describe coupling matrices within the principal unit cells (intralayer), with odd and even indices n, respectively, and H_{AB} denotes the effective coupling between two adjacent unit cells (interlayer) based on the tight-binding model given by Eq. (1).

The calculated band structures of ZBLPNR with $N = 24$ for various gate voltages are shown in Fig. 2. In similarity with a zigzag phosphorene nanoribbon (ZPNR), the ZBLPNR has two nearly degenerate quasiflat-edge modes at the Fermi level [70–74] that are entirely detached from the bulk bands. The degeneracy of these two quasiflat bands is broken by applying a perpendicular electric field. The properties of edge states in ZBLPNRs are essentially different from the other 2D zigzag nanoribbons. In comparison with ZBLPNR and ZPNR, in 2D Dirac materials such as graphene and silicene, the edge modes merge into the bulk bands at the two Dirac points. As recently addressed by Ezawa [71], the origin of this decoupling matter of the flat edge modes is the presence of

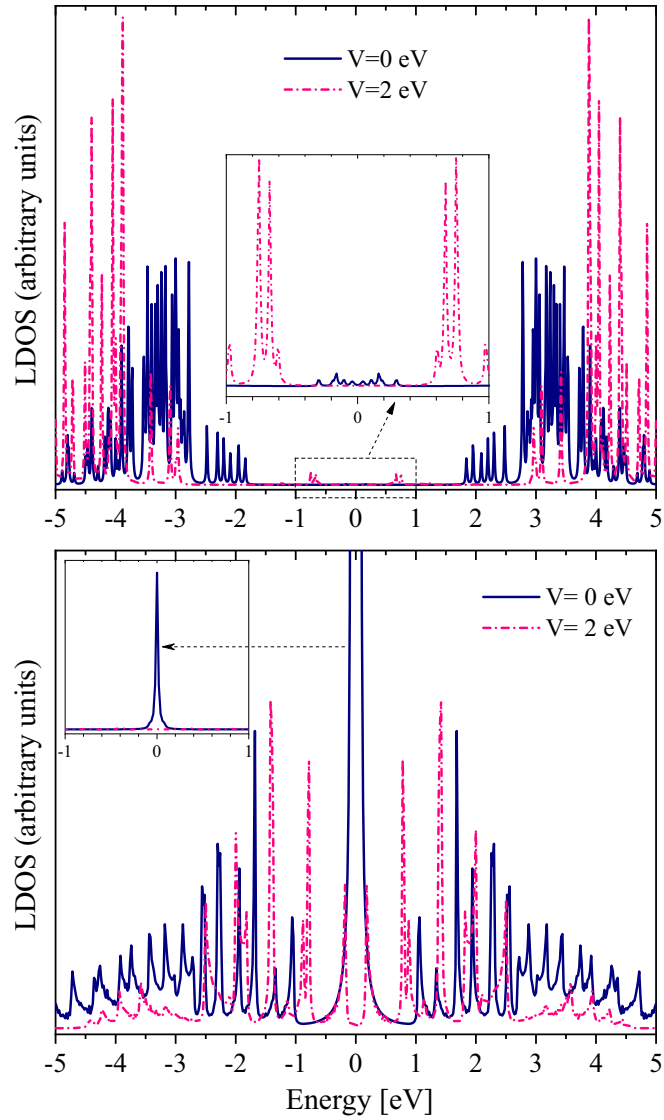

FIG. 3. Site-resolved local densities of states (LDOS) calculated for ZBLPNR with $M = 300$ and $N = 24$. Top panel: for a bulk site with coordinate (150,12) and bottom panel: for an edge site with coordinate (150,1). For better clarity, the LDOS within an energy range of -1 to 1 eV is shown in the insets. In contrast to the bulk LDOS (top panel), when the applied gate voltage is zero ($V = 0$), the edge LDOS (bottom panel) shows a sharp peak around zero energy corresponding to the edge states (see insets).

two out-of-plane zigzag chains, coupled by a relatively strong hopping parameter.

The energy dispersion and wave functions can also be obtained by numerical diagonalization of the nearest-neighbor tight-binding model Hamiltonian given by Eq. (1). To calculate the site-resolved local density of states (LDOS) for the ith site of the ribbon as $\rho_i(\mathbf{r}, E) = -\frac{1}{\pi}\mathrm{Im}[G_{ii}(\mathbf{r}, \mathbf{r}, E)]$, the corresponding wave function for a given energy and wave vector should first be obtained. $G_{ii}(\mathbf{r}, \mathbf{r}, E)]$ is the real-space Green's function at the ith site. Figure 3 displays the LDOS of phosphorus atoms in sublattices either at the edge or in the bulk. The top and bottom panels present the LDOSs of the bulk and the edge sites at the sublattices (150,12) and (150,1),

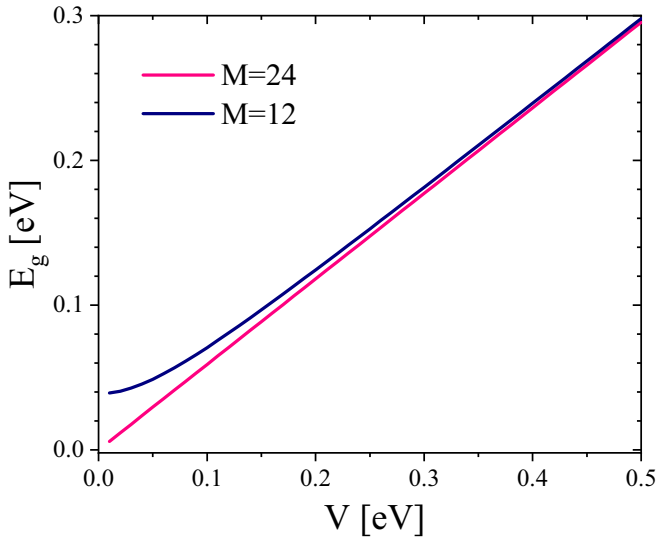

FIG. 4. Energy gap of bilayer phosphorene nanoribbons with widths $N = 12, 24$ as a function of the perpendicular electric potential.

respectively. We note that in contrast to the bulk LDOS, when the applied gate voltage is zero, the edge LDOS shows a sharp peak around zero energy corresponding to edge states. This unique property is also seen in the LDOS profile of the ZPNR [75].

Moreover, Fig. 4 shows the energy gap E_g of the ZBLPNR for two different ribbon widths ($N = 12, 24$) as a function of the applied electric field. As previously obtained, the energy gap increases linearly as the applied electric field is increased [23]. The zero-biased gap decreases with increasing ribbon width and tends to zero in the limit of very large N.

The carrier-mediated exchange coupling between the spin of itinerant electrons and two magnetic impurities with magnetic moments $\mathbf{S}_1$ and $\mathbf{S}_2$, located, respectively, at $\mathbf{r}$ and $\mathbf{r}'$, is given by

$$V = -\lambda[\mathbf{S}_1 \cdot \mathbf{s}(\mathbf{r}) + \mathbf{S}_2 \cdot \mathbf{s}(\mathbf{r}')], \tag{3}$$

where $\mathbf{s}(\mathbf{r})$, $\mathbf{s}(\mathbf{r}')$ are the conduction electron spin densities at positions $\mathbf{r}$ and $\mathbf{r}'$, respectively, and λ is the coupling between the impurity spins and the itinerant carriers.

In the linear-response regime, the interaction energy between the two localized magnetic moments may be written in Heisenberg form [40–42,76],

$$E(\mathbf{r}, \mathbf{r}') = J(\mathbf{r}, \mathbf{r}')\, \mathbf{S}_1 \cdot \mathbf{S}_2. \tag{4}$$

The RKKY interaction $J(\mathbf{r}, \mathbf{r}')$ is explained using the susceptibility, the response of the charge density n to a perturbing potential V,

$$J(\mathbf{r}, \mathbf{r}') = \frac{\lambda^2 \hbar^2}{4} \chi(\mathbf{r}, \mathbf{r}'), \tag{5}$$

where $\chi(\mathbf{r}, \mathbf{r}') \equiv \delta n(\mathbf{r})/\delta V(\mathbf{r}')$ is the charge susceptibility for a crystal, $\delta V(r')$ is a spin-independent perturbing potential, and $\delta n(\mathbf{r})$ is the induced charge density.

The static spin susceptibility can be written in terms of the integral over the unperturbed Green's function,

$$\chi(\mathbf{r}, \mathbf{r}') = -\frac{2}{\pi} \int_{-\infty}^{\varepsilon_F} d\varepsilon\, \mathrm{Im}[G^0(\mathbf{r}, \mathbf{r}', \varepsilon) G^0(\mathbf{r}', \mathbf{r}, \varepsilon)], \tag{6}$$

where ε_F is the Fermi energy. The expression for the susceptibility may be obtained by using the spectral representation of the Green's function,

$$G^0(\mathbf{r}, \mathbf{r}', \varepsilon) = \sum_{n,s} \frac{\psi_{n,s}(\mathbf{r}) \psi^*_{n,s}(\mathbf{r}')}{\varepsilon + i\eta - \varepsilon_{n,s}}, \tag{7}$$

where $\psi_{n,s}$ is the sublattice component of the unperturbed eigenfunction with the corresponding energy $\varepsilon_{n,s}$. For a crystalline structure, n, s denotes the band index and spin. In other words, it denotes a complete set of quantum states. Substituting Eq. (7) into Eq. (6), we obtain the result

$$\begin{aligned}
&\chi(\mathbf{r}, \mathbf{r}') \\
&= -\frac{2}{\pi} \int_{-\infty}^{\varepsilon_F} d\varepsilon \sum_{\substack{n,s \\ n',s'}} \{\mathrm{Re}\,[\psi_{n,s}(\mathbf{r}) \psi^*_{n,s}(\mathbf{r}') \psi_{n',s'}(\mathbf{r}') \\
&\quad \times \psi^*_{n',s'}(\mathbf{r})] \mathrm{Im}[(\varepsilon + i\eta - \varepsilon_{n,s})(\varepsilon + i\eta - \varepsilon_{n',s'})]^{-1} \\
&\quad + \mathrm{Im}[\psi_{n,s}(\mathbf{r}) \psi^*_{n,s}(\mathbf{r}') \psi_{n',s'}(\mathbf{r}') \psi^*_{n',s'}(\mathbf{r})] \\
&\quad \times \mathrm{Re}[(\varepsilon + i\eta - \varepsilon_{n,s})(\varepsilon + i\eta - \varepsilon_{n',s'})]^{-1}\}.
\end{aligned} \tag{8}$$

After exchanging the dummy variables n, s with n', s', the imaginary part of the product of the four wave functions appearing in the equation above is odd while its real part is even, and at the same time both the imaginary and the real parts of the product of the energy-space Green's function are even. By applying this property, the second expression becomes zero. Finally, $\chi(\mathbf{r}, \mathbf{r}')$ reads

$$\begin{aligned}
\chi(\mathbf{r}, \mathbf{r}') = &\sum_{\substack{n,s \\ n',s'}} \psi_{n,s}(\mathbf{r}) \psi^*_{n,s}(\mathbf{r}') \psi_{n',s'}(\mathbf{r}') \psi^*_{n',s'}(\mathbf{r}) \\
&\times \mathcal{E}(n, s, n', s'),
\end{aligned} \tag{9}$$

in which

$$\mathcal{E}(n, s, n', s') = 2 \int_{-\infty}^{\varepsilon_F} d\varepsilon \left[\frac{\delta(\varepsilon - \varepsilon_{n',s'})}{\varepsilon - \varepsilon_{n,s}} + \frac{\delta(\varepsilon - \varepsilon_{n,s})}{\varepsilon - \varepsilon_{n',s'}} \right]. \tag{10}$$

To prove the above equality, we use the relationship $\lim_{\eta \to 0^+} (x \pm i\eta)^{-1} = \mathcal{P}(1/x) \mp i\pi\delta(x)$. The integration over energy can be carried out next, leading to our desired result,

$$\begin{aligned}
\chi(\mathbf{r}, \mathbf{r}') = 2 \sum_{\substack{n,s \\ n',s'}} &\left[\frac{f(\varepsilon_{n,s}) - f(\varepsilon_{n',s'})}{\varepsilon_{n,s} - \varepsilon_{n',s'}} \right. \\
&\left. \times \psi_{n,s}(\mathbf{r}) \psi^*_{n,s}(\mathbf{r}') \psi_{n',s'}(\mathbf{r}') \psi^*_{n's'}(\mathbf{r}) \right],
\end{aligned} \tag{11}$$

where $f(\varepsilon)$ is the Fermi function. The above equation is a well-known formula in the linear-response theory that is the main equation in this work. It is worth noting that after interchanging the n, s and n', s' indices, the summand in

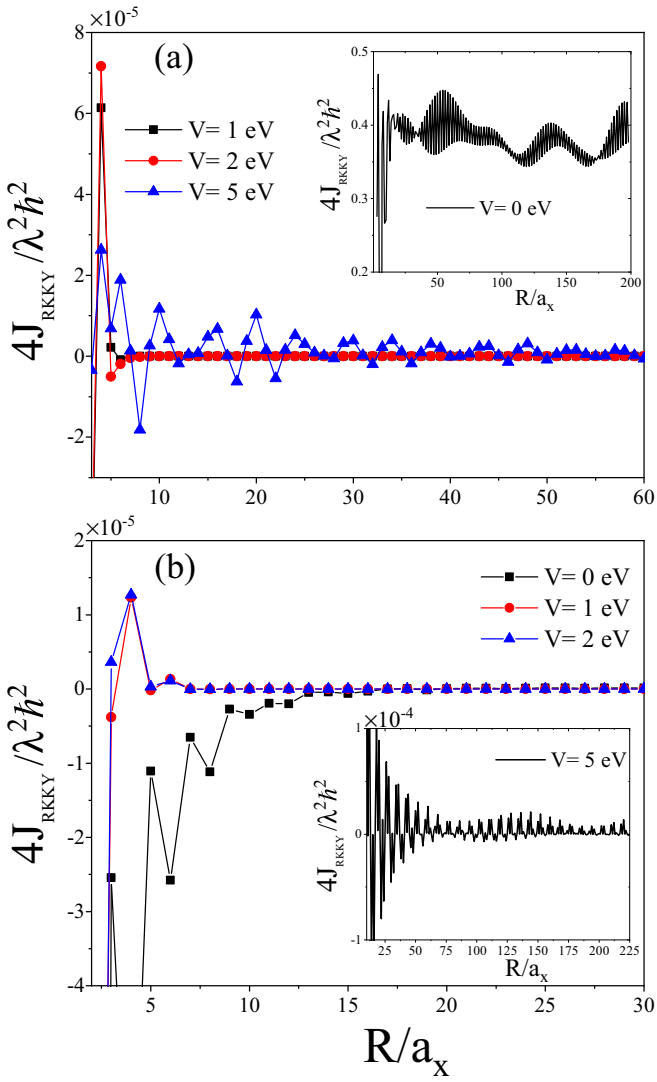

FIG. 5. Scaled RKKY interaction as a function of the impurity distance for the ZBLPNR with $M = 300$ and $N = 24$. (a) Impurities located on the same edge such that the first impurity is fixed at the sublattice (10,1) and the second one is located at $(m, 1)$, where $m = 11, 12, 13, \ldots$. As in the absence of the electric potential, the strength of the RKKY interaction is approximately five orders of magnitude larger than the biased ZBLPNR; we show the result for $V = 0$ in the inset. (b) Impurities located inside the ZBLPNR such that the first impurity is located on the sublattice (10,12) and the second one is placed at $(m, 12)$, with $m = 11, 12, 13, \ldots$ for various electric potentials. For better clarity, we show the result for $V = 5$ eV in the inset.

Eq. (11) converts to its complex conjugate, so that only the real part survives.

III. NUMERICAL RESULTS

In this section, we present our main results for the exchange coupling in the zigzag bilayer phosphorene nanoribbon as well as its tunability via the perpendicular electric voltage. To do so, we evaluate the static spin susceptibility Eq. (11) in real space in various configurations of the magnetic impurities at various bias voltages.

Figure 5 shows the spatial behavior of the RKKY interaction for two impurities: (a) both sitting on the same edge along the line $n = 1$, and (b) both located inside the zigzag nanoribbon (away from the edges) along the line $n = 12$ for different bias voltages for a ZBLPNR with $M = 300, N = 24$. As indicated, in the case of both impurities located at the edge (top panel), at low voltage the RKKY interaction displays oscillatory behavior in R and decays fast with short-ranged behavior. More interestingly, by increasing the electric field, the RKKY interaction strength is dramatically quenched, as can be seen in the zero-bias limit ($V \simeq 0$), i.e., the RKKY interaction is about five orders of magnitude larger than the nonzero-bias regime ($V \neq 0$). The reason for that is related to the existence of nearly-zero-energy states at the edges of the ZBLPNR. In the high-field regime ($V = 5$ eV), the RKKY interaction exhibits long-range oscillatory behavior in R, because the Fermi energy crosses the bulk bands. Similar to the ZPNR [75], the RKKY coupling attains its maximum strength when the applied gate voltage is zero. The contribution of the bulk states is nearly zero as the impurities are located at the edge of the ZBLPNR.

Otherwise, when two impurity atoms are located in the interior region of the ZBLPNR, no difference in the order of magnitude appears for different bias voltages [see Fig. 5(b)]. As can be seen, RKKY shows a few oscillations in R, and then it decays fast with short-ranged behavior. More interestingly, in the presence of a large bias potential ($V = 5$ eV), a beating pattern of oscillations of the RKKY interaction occurs when two magnetic impurities are located inside the ZBLPNR. The beating feature originates mainly from the bulk bands crossing the Fermi level for the bulk impurities, where both moments are located inside the ZBLPNR.

To explore the spatial dependence of the RKKY interaction, we have presented the log-log plots in Fig. 6 for the ZBLPNR with $M = 300, N = 24$. (a) Impurities are located on the edge such that the first impurity is fixed at the sublattice (10,1) and the second one is located at $(m, 1)$, and (b) impurities are located inside the ZBLPNR such that the first and second impurities are fixed at the sublattices (10,12) and $(m, 12)$, respectively, where $m = 11, 12, 13, \ldots$. The dashed-red lines show the slopes corresponding to the relevant decay rates, and the black-solid lines show the log of the RKKY coupling. The cases of (a) and (b) represent a decay rate of R^{-5} and R^{-3}, respectively. Hence, the RKKY interaction for impurities located on the edge decays faster than the interaction of the impurities located inside the region of the ZBLPNR. The position and direction dependence arise from quantum interference effects caused by the boundary conditions imposed on the electronic structure of the nanoribbon [77,78].

Figure 7 shows the spatial behavior of the RKKY interaction when the first impurity is fixed at the edge at sublattice (150,1) and the second one is moved along the line $m = 150$ with coordinates $(150, n)$, where $n = 2, 3, \ldots, 24$. As in the absence of applied bias ($V = 0$) the exchange coupling is approximately two orders of magnitude greater than the case with potential ($V \neq 0$), for better clarity we multiply the values related to zero bias by 10^{-2}. In the case of zero

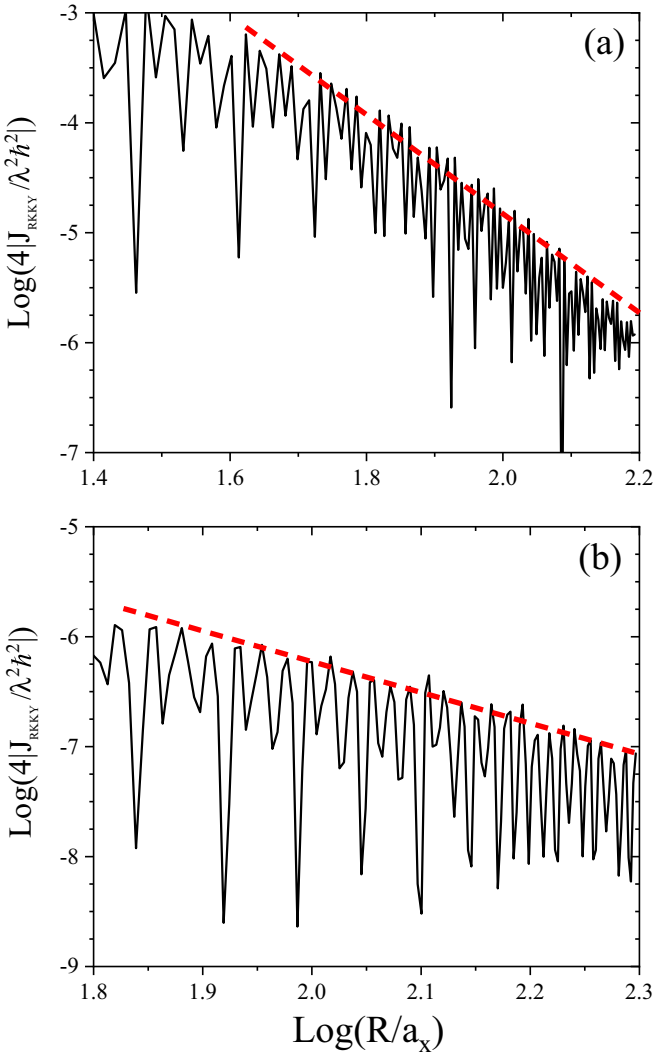

FIG. 6. A log-log plot of the numerical results of the scaled RKKY interaction as a function of the impurity distance for the ZBLPNR for $M = 300$ and $N = 24$. (a) Both impurities are at the edge such that the first impurity is fixed at the sublattice (10,1) and the second one is located at $(m, 1)$, and (b) impurities located inside the ZBLPNR such that the first impurity is fixed at the sublattice (10,12) and the second one is located at $(m, 12)$, where $m = 11, 12, 13, \ldots$. The solid-black lines show the log of the RKKY coupling, and the dashed-red lines represent the relevant decay rates. The cases of (a) and (b) represent a decay rate of R^{-5} and R^{-3}, respectively.

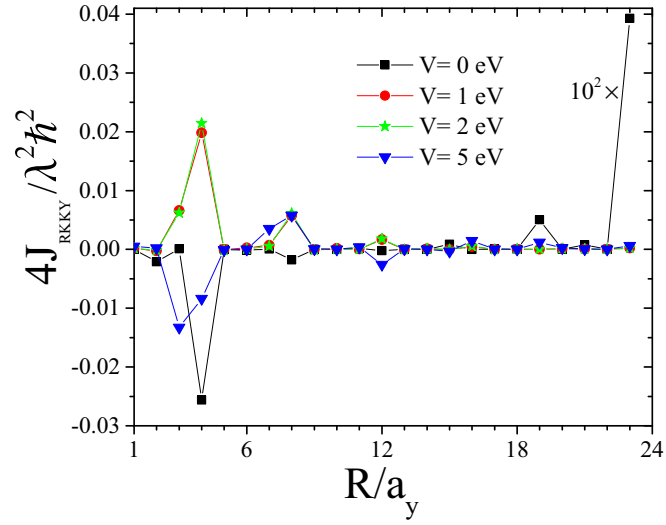

FIG. 7. Scaled RKKY interaction as a function of the impurity distance for the ZBLPNR with $M = 300$ and $N = 24$, when the first impurity is fixed at the edge at sublattice (150,1), and the second one is moved along the armchair line $m = 150$ with coordinates $(150, n)$, with $n = 2, 3, \ldots, 24$.

bias, for both impurities located at an armchair chain (both located in the same ZBLPNR unit cell), the largest coupling appears when both moments are located at two counterpart edge sublattices.

Figures 8(a)–8(d) show the numerical results for the RKKY coupling as a function of the bias voltage for different configurations of magnetic impurities. Figure 8(a) shows when two impurities are fixed at the same zigzag edge at (146,1) and (151,1) lattice points. Turning on the electric field, a sudden falloff in the RKKY interaction strength occurs because the zero-energy state at the edge of the ZBLPNR is suddenly dropped. This behavior is also attainable for moments located at two counterpart edge sublattices [Fig. 8(d)] because by turning on the electric field, the edge modes in ZBLPNR become fully separated from the bulk. This unique nature of the edge states in ZBLPNR allows us to probe them separately from the bulk.

Numerical results for when the first impurity is fixed at the zigzag edge at (146,1) and the second one is located inside the ZBLPNR at the (146,12) lattice point are shown in Fig. 8(b). Figure 8(c) shows the RKKY coupling for two impurities fixed inside the ZBLPNR at (146,12) and (151,12) lattice points.

IV. SUMMARY

We study the Ruderman-Kittel-Kasuya-Yosida (RKKY) interaction between local magnetic moments in zigzag bilayer phosphorene nanoribbons (ZBLPNRs) placed under a perpendicular electric field. For this, we evaluate the spatial and electric field dependency of the static spin susceptibility in real space in various configurations of magnetic impurities at zero temperature. We evaluate this interaction from a Green's-function approach based on the tight-binding model Hamiltonian. For large distances, the RKKY interaction falls off as R^{-5} for moments located on the zigzag edge, whereas for those placed in the interstitial sites they decay as R^{-3}. The electrically tunable RKKY interaction of ZBLPNRs is expected to have important consequences on the spintronic application of biased ZBLPNRs. As shown, the signatures of these unique quasiflat-edge modes in ZBLPNRs could be explored by using the RKKY interaction. Due to the existence of quasiflat bands at the Fermi level, in the absence of an electric field, a sharp peak in the RKKY interaction is seen. In the presence of a large bias potential, a beating pattern of oscillations of the RKKY interaction occurs when two magnetic impurities are located inside the ZBLPNR.

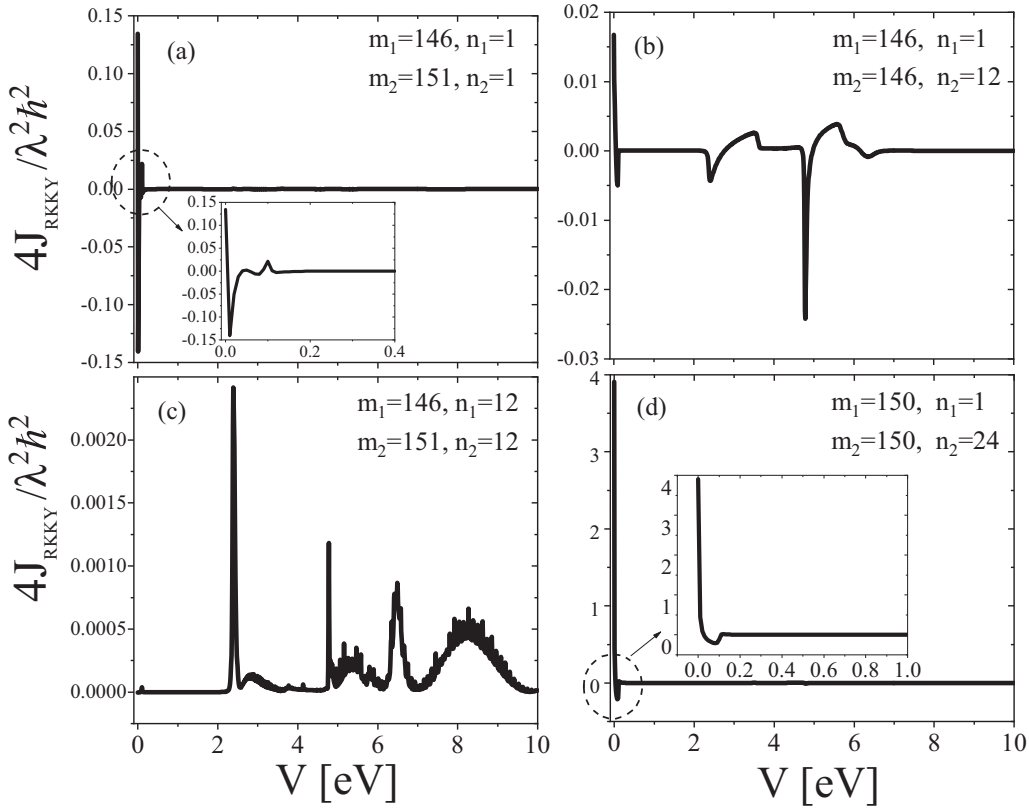

FIG. 8. Scaled RKKY interaction as a function of the perpendicular electric potential for $M = 300$ and $N = 24$, when (a) both impurities are fixed at the zigzag edge at (146,1) and (151,1) lattice points, (b) the first impurity is fixed at the zigzag edge at (150,1) and the second one is located inside the ZBLPNR at the (150,12) lattice point, (c) both impurities are located inside the ZBLPNR at (146,12) and (151,12) lattice points, and (d) impurities are fixed at the counterpart zigzag edges at (146,1) and (146,24) lattice points.

The electronic properties of the ZBLPNR in the presence of gate voltage are also obtained. In comparison to other 2D materials such as graphene, silicene, etc., ZBLPNRs have two nearly degenerate quasiflat-edge modes at the Fermi level of the ZBLPNR, isolated from the bulk states. A gap occurs by applying a perpendicular electric field. By varying the width of the phosphorene ribbons, we find that the size effect is crucial for determining the relative importance of the edge state. As previously obtained [23], the energy gap increases linearly as the applied electric field is increased. The zero-bias gap decreases with increasing ribbon width and tends to zero in the limit of very large N.

ACKNOWLEDGMENT

This work is partially supported by Iran Science Elites Federation.

[1] L. Li, Y. Yu, G. J. Ye, Q. Ge, X. Ou, H. Wu, D. Feng, X. H. Chen, and Y. Zhang, Nat. Nanotechnol. **9**, 372 (2014).
[2] H. Liu, A. T. Neal, Z. Zhu, Z. Luo, X. Xu, D. Tomanek, and P. D. Ye, ACS Nano **8**, 4033 (2014).
[3] A. Castellanos-Gomez, Nat. Photon. **10**, 202 (2016).
[4] F. Xia, H. Wang, D. Xiao, M. Dubey, and A. Ramasubramaniam, Nat. Photon. **8**, 899 (2014).
[5] M. Zare, L. Majidi, and R. Asgari, Phys. Rev. B **95**, 115426 (2017).
[6] A. Carvalho, M. Wang, X. Zhu, A. S. Rodin, H. Su, and A. H. Castro Neto, Nat. Rev. Mater. **1**, 16061 (2016).
[7] M. Batmunkh, M. Bat-Erdene, and J. Shapter, Adv. Mater. **28**, 8586 (2016).
[8] H. Liu, Y. Du, Y. Deng, and P. D. Ye, Chem. Soc. Rev. **44**, 2732 (2015).
[9] S. Das, M. Demarteau, and A. Roelofs, ACS Nano **8**, 11730 (2014).
[10] M. V. Kamalakar, B. N. Madhushankar, A. Dankert, and S. P. Dash, Small **11**, 2209 (2015).
[11] W. Lu, H. Nan, J. Hong, Y. Chen, C. Zhu, Z. Liang, X. Ma, Z. Ni, C. Jin, and Z. Zhang, Nano Res. **7**, 853 (2014).
[12] R. Fei and L. Yang, Nano Lett. **14**, 2884 (2014).
[13] X. Wang, A. M. Jones, K. L. Seyler, V. Tran, Y. Jia, H. Zhao, H. Wang, L. Yang, X. Xu, and F. Xia, Nat. Nanotechnol. **10**, 517 (2015).
[14] M. Zare, B. Z. Rameshti, F. G. Ghamsari, and R. Asgari, Phys. Rev. B **95**, 045422 (2017).

[15] V. Tran, R. Soklaski, Y. Liang, and L. Yang, Phys. Rev. B **89**, 235319 (2014).
[16] Y. Du, C. Ouyang, S. Shi, and M. Lei, J. Appl. Phys. **107**, 093718 (2010).
[17] D. Çakir, H. Sahin, and F. M. Peeters, Phys. Rev. B **90**, 205421 (2014).
[18] L. Liang, J. Wang, W. Lin, B. G. Sumpter, V. Meunier, and M. Pan, Nano Lett. **14**, 6400 (2014).
[19] A. S. Rodin, A. Carvalho, and A. H. Castro Neto, Phys. Rev. Lett. **112**, 176801 (2014).
[20] I. Zutić, J. Fabian, and S. D. Sarma, Rev. Mod. Phys. **76**, 323 (2004).
[21] R. Babar and M. Kabir, J. Phys. Chem. C **120**, 1491 (2016).
[22] H. Zheng, J. Zhang, B. Yang, X. Du, and Y. Yan, Phys. Chem. Chem. Phys. **17**, 16341 (2015).
[23] L. Yang, W. Mi, and X. Wang, J. Alloys Compd. **662**, 528 (2016).
[24] I. Khan and J. Hong, New J. Phys. **17**, 023056 (2015).
[25] Z. Zhu, C. Li, W. Yu, D. Chang, Q. Sun, and Y. Jia, Appl. Phys. Lett. **105**, 113105 (2014).
[26] Y. Du, H. Liu, B. Xu, L. Sheng, J. Yin, C.-G. Duan, and X. Wan, Sci. Rep. **5**, 8921 (2015).
[27] M. U. Farooq, A. Hashmi, and J. Hong, ACS Appl. Mater. Interf. **7**, 14423 (2015).
[28] M. U. Farooq, A. Hashmi, and J. Hong, Sci. Rep. **6**, 26300 (2016).
[29] G. Yang, S. Xu, W. Zhang, T. Ma, and C. Wu, Phys. Rev. B **94**, 075106 (2016).
[30] P. Srivastava, K. Hembram, H. Mizuseki, K. Lee, S. Han, and S. Kim, J. Phys. Chem. C **119**, 6530 (2015).
[31] N. Suvansinpan, F. Hussain, G. Zhang, C. Chiu, Y. Cai, and Y.-W. Zhang, Nanotechnology **27**, 065708 (2016).
[32] C. Zhai, X. Dai, W. Li, Y. Ma, T. Wang, and Y. Tang, Superlattices Microstruct. **101**, 49 (2017).
[33] I. Khan and J. Hong, Nanotechnology **27**, 385701 (2016).
[34] V. V. Kulish, O. I. Malyi, C. Persson, and P. Wu, Phys. Chem. Chem. Phys. **17**, 992 (2014).
[35] L. Seixas, A. Carvalho, and A. H. Castro Neto, Phys. Rev. B **91**, 155138 (2015).
[36] X. Sui, C. Si, B. Shao, X. Zou, J. Wu, B.-L. Gu, and W. Duan, J. Phys. Chem. C **119**, 10059 (2015).
[37] T. Hu and J. Hong, J. Phys. Chem. C **119**, 8199 (2015).
[38] W. Yu, Z. Zhu, C. Niu, C. Li, J. Cho, and Y. Jia, Nanoscale Res. Lett. **11**, 77 (2016).
[39] X. Cai, C. Niu, J. Wang, W. Yu, X. Ren, and Z. Zhu, Phys. Lett. A **381**, 1236 (2017).
[40] M. A. Ruderman and C. Kittel, Phys. Rev. **96**, 99 (1954).
[41] T. Kasuya, Prog. Theor. Phys. **16**, 45 (1956).
[42] K. Yosida, Phys. Rev. **106**, 893 (1957).
[43] M. A. H. Vozmediano, M. P. Lopez-Sancho, T. Stauber, and F. Guinea, Phys. Rev. B **72**, 155121 (2005).
[44] L. Brey, H. A. Fertig, and S. Das Sarma, Phys. Rev. Lett. **99**, 116802 (2007).
[45] D. J. Priour, E. H. Hwang, and S. Das Sarma, Phys. Rev. Lett. **92**, 117201 (2004).
[46] F. Matsukura, H. Ohno, A. Shen, and Y. Sugawara, Phys. Rev. B **57**, 2037(R) (1998).
[47] K. T. Ko, K. Kim, S. B. Kim, H. D. Kim, J. Y. Kim, B. I. Min, J. H. Park, F. H. Chang, H. J. Lin, A. Tanaka, and S. W. Cheong, Phys. Rev. Lett. **107**, 247201 (2011).
[48] H. Ohno, Science **281**, 951 (1998).
[49] E. Minamitani, W. A. Dino, H. Nakanishi, and H. Kasai, Phys. Rev. B **82**, 153203 (2010).
[50] C.-H. Hsu, P. Stano, J. Klinovaja, and D. Loss, Phys. Rev. B **92**, 235435 (2015).
[51] M. Zare, F. Parhizgar, and R. Asgari, Phys. Rev. B **94**, 045443 (2016).
[52] M. Shiranzaei, H. Cheraghchi, and F. Parhizgar, Phys. Rev. B **96**, 024413 (2017).
[53] D. A. Abanin and D. A. Pesin, Phys. Rev. Lett. **106**, 136802 (2011).
[54] P. J. T. Eggenkamp, H. J. M. Swagten, T. Story, V. I. Litvinov, C. H. W. Swüste, and W. J. M. de Jonge, Phys. Rev. B **51**, 15250 (1995).
[55] F. S. Liu, W. A. Roshen, and J. Ruvalds, Phys. Rev. B **36**, 492 (1987).
[56] F. Parhizgar, M. Sherafati, R. Asgari, and S. Satpathy, Phys. Rev. B **87**, 165429 (2013).
[57] F. Parhizgar, H. Rostami, and R. Asgari, Phys. Rev. B **87**, 125401 (2013).
[58] F. Parhizgar, R. Asgari, S. Abedinpour, and M. Zareyan, Phys. Rev. B **87**, 125402 (2013).
[59] M. Sherafati and S. Satpathy, Phys. Rev. B **83**, 165425 (2011).
[60] M. Shiranzaei, F. Parhizgar, J. Fransson, and H. Cheraghchi, Phys. Rev. B **95**, 235429 (2017).
[61] J. Klinovaja and D. Loss, Phys. Rev. B **87**, 045422 (2013).
[62] R. A. Moslem Zare and F. Parhizgar, J. Magn. Magn. Mater. **456**, 307 (2018).
[63] H. Duan, S. Li, S.-H. Zheng, Z. Sun, M. Yang, and R.-Q.Wang, New J. Phys. **19**, 103010 (2017).
[64] L. L. Li, D. Moldovan, W. Xu, and F. M. Peeters, Phys. Rev. B **96**, 155425 (2017).
[65] D. Çakir, C. Sevik, and F. M. Peeters, Phys. Rev. B **92**, 165406 (2015).
[66] B. Jhun and C.-H. Park, Phys. Rev. B **96**, 085412 (2017).
[67] A. N. Rudenko, S. Yuan, and M. I. Katsnelson, Phys. Rev. B **92**, 085419 (2015).
[68] K. Dolui and S. Quek, Sci. Rep. **5**, 11699 (2015).
[69] S. Yuan, E. van Veen, M. I. Katsnelson, and R. Roldan, Phys. Rev. B **93**, 245433 (2016).
[70] A. Maity, A. Singh, P. Sen, A. Kibey, A. Kshirsagar, and D. G. Kanhere, Phys. Rev. B **94**, 075422 (2016).
[71] M. Ezawa, New J. Phys. **16**, 115004 (2014).
[72] E. T. Sisakht, M. H. Zare, and F. Fazileh, Phys. Rev. B **91**, 085409 (2015).
[73] R. Ma, H. Geng, W. Y. Deng, M. N. Chen, L. Sheng, and D. Y. Xing, Phys. Rev. B **94**, 125410 (2016).
[74] B. Ostahie and A. Aldea, Phys. Rev. B **93**, 075408 (2016).
[75] SK Firoz Islam, Paramita Dutta, A. M. Jayannavar, and Arijit Saha, Phys. Rev. B **97**, 235424 (2018).
[76] H. Imamura, P. Bruno, and Y. Utsumi, Phys. Rev. B **69**, 121303(R) (2004).
[77] D. F. Kirwan, C. G. Rocha, A. T. Costa, and M. S. Ferreira, Phys. Rev. B **77**, 085432 (2008).
[78] S. R. Power, V. M. de Menezes, S. B. Fagan, and M. S. Ferreira, Phys. Rev. B **84**, 195431 (2011).